Lifetimes and timescales of tropospheric ozone

Michael J. Prather and Xin Zhu

Department of Earth System Science, University of California at Irvine, Irvine, CA 92697-3100, USA
Correspondence to: Michael J. Prather (mprather@uci.edu)

Abstract

The lifetime of tropospheric O_3 is difficult to quantify because we model O_3 as a secondary pollutant, without direct emissions. For other reactive greenhouse gases like CH_4 and N_2O, we readily model lifetimes and timescales that include chemical feedbacks based on direct emissions. Here, we devise a set of artificial experiments with a chemistry-transport model where O_3 is directly emitted into the atmosphere at a quantified rate. We create three primary emission patterns for O_3, mimicking secondary production by surface industrial pollution, that by aviation, and primary injection through stratosphere-troposphere exchange (STE). The perturbation lifetimes for these O_3 sources includes chemical feedbacks and varies from 6 to 27 days depending on source location and season. Previous studies derived lifetimes around 24 days estimated from the mean odd-oxygen loss frequency. The timescales for decay of excess O_3 varies from 10–20 days in NH summer to 30–40 days in NH winter. For each season, we identify a single O_3 chemical mode applying to all experiments. Understanding how O_3 sources accumulate (the lifetime) and disperse (decay timescale) provides some insight into how changes in pollution emissions, climate, and stratospheric O_3 depletion over this century will alter tropospheric O_3. This work incidentally found two distinct mistakes in how we diagnose tropospheric O_3, but not how we model it. First, the chemical pattern of an O_3 perturbation or decay mode does not resemble our traditional view of the odd-oxygen family of species that includes NO_2. Instead, a positive O_3 perturbation is accompanied by a decrease in NO_2. Second, heretofore we diagnosed the importance of STE flux to tropospheric O_3 with a synthetic 'tagged' tracer O3S, which had full stratospheric chemistry and linear tropospheric loss based on odd-oxygen loss rates. These O3S studies predicted that about 40 % of tropospheric O_3 was of stratospheric origin, but our lifetime and decay experiments show clearly that STE fluxes add about 8 % to tropospheric O_3, providing further evidence that tagged tracers do not work when the tracer is a major species with chemical feedbacks on its loss rates, as shown for CH_4.

1. Introduction

Ozone (O_3) is an essential but dangerous component of the atmosphere and the air we breathe. Tropospheric ozone is detrimental to human and plant health and also responsible for about 12% of the greenhouse-gas driven climate change to date (Szopa et al 2021); yet, it is essential as the primary source of hydroxyl radicals (OH) that cleanse the lower atmosphere of many pollutants (Levy, 1972). The total ozone column, predominantly stratospheric, shields us from ultraviolet-B that damages skin cells (Roffo, 1939; Blum, 1959). The natural chemistry of stratospheric O_3 and its catalytic depletion by a range of anthropogenic trace gases is well recognized (Chapman, 1930; Bates and Nicolet, 1950; Junge, 1962; Danielsen, 1968; Johnston, 1971; Molina and Rowland, 1974; WMO, 2022). In the troposphere, O_3 is a secondary pollutant meaning that it is produced chemically from other pollutants (Haagen-Smit, 1952; Haagen-Smit and Fox, 1955; Chameides and Walker, 1973; Fishman and Crutzen, 1978; Logan et al., 1981). Because of this lack of direct emissions, our understanding and modeling of O_3 is quite different from that of other chemical pollutants and greenhouse gases. For example, we do not create atmospheric budgets tied to emissions, and thus we do not derive lifetimes as we do for other gases like methane (CH_4) based on the atmospheric burden divided by emissions. Here, we take a new approach to the study of

tropospheric O_3 by simulating a direct emission source of O_3 and then following its perturbation on the background atmosphere to derive that source's lifetime and thence the timescale to remove that excess O_3.

We study the perturbation to O_3 from hypothesized primary emissions associated with (i) surface industrial pollution, (ii) aviation, and (iii) stratosphere-troposphere exchange using the UC Irvine chemistry-transport model (UCI CTM) with stratospheric-plus-tropospheric chemistry. A 3D emission pattern with 100 Tg-O_3 yr^{-1} is maintained in these experiments. We diagnose the pattern and burden of excess O_3 over different meteorological years. Nominally, we would calculate the 'lifetime' of tropospheric O_3 following the standard definition: global O_3 burden (Tg) at steady state divided by total emissions or total losses (Tg yr^{-1}). The budget-based lifetime for a trace gas like methyl bromide (CH_3Br) is based on the burden in all connected reservoirs (i.e., stratosphere, troposphere, ocean mixed layer) (Butler, 1994), but this will not work for tropospheric O_3. The quantity derived here is the 'perturbation lifetime' since we ratio the excess burden to the excess emissions. Note that the perturbation lifetime includes the chemical feedbacks, which the global lifetime does not, e.g., the CH_4 perturbation lifetime is about 1.4 times larger than the global lifetime because of methane's feedback on its chemical loss rate (Isaksen and Hov, 1987).

We follow the decay of the excess O_3 after emissions are cut and calculate a timescale for the O_3 perturbation from the long-term e-fold rate. The timescale is nominally that of the longest-lived chemical mode involving tropospheric O_3, which is an inherent property of the atmosphere; whereas the lifetime depends on the location of emissions because the emissions are exposed to different photochemical activity. This relationship between lifetimes and timescales is well known for CH_4 (Isaksen and Hov, 1987; Prather, 1994, 1996), CH_3Br (Butler, 1994; Prather, 1997) and other gases (Prather, 2007), but has not yet been explored for tropospheric O_3. Because chemical feedbacks are included in both the temporal decay and the perturbation lifetime, both values are expected to be similar.

The experimental design, O_3 chemistry, and specific experiments are presented in Section 2. The steady-state lifetime and patterns are analysed in Section 3. The decay patterns and timescales are given in Section 4. The results here are inconsistent with some conclusions about the stratospheric influence on tropospheric O_3 using tagged tracers like O3S (Follows and Austin, 1992), and these are discussed with the conclusions about O_3 lifetime and timescales in Section 5.

2. Methods

2.1. Defining production and loss of tropospheric O_3

In current chemistry-climate or chemistry-transport models (CCMs or CTMs), the chemical continuity equation for O_3 is usually calculated correctly using all the rates directly involving O_3. The local, grid-cell equation for O_3 chemical tendency looks like

$$d[O_3]/dt = + k(T,M)\,[O]\,[O_2] - J(O_3)\,[O_3] - k(T)\,[O_3]\,[NO] - k(T)\,[O_3]\,[HO_2] - \ldots \quad (1)$$

where all chemical reactions directly involving $[O_3]$ are included. Because of the rapid exchange of O and O_3, the first three terms largely cancel one another; and the timescales of the system are not represented by the negative loss terms divided by $[O_3]$. For example, the photolysis frequency $J(O_3)$ does not represent any of the timescales of the O_3-O system as shown in the eigenvalue decomposition of Chapman O_3 chemistry (Section 3 of Prather, 2007). The desire to remove these large rates from the O_3 chemical budget, in part to estimate a more realistic loss rate and timescale, has led to complex definitions of the family grouping called odd oxygen,

$$O_X \equiv O_3 + O + NO_2 + 2\,x\,NO_3 + \ldots \quad (2)$$

Because O_3 is the dominant species in the O_X family, the loss of O_X is expected to represent the lifetime and timescales of O_3 in the stratosphere or troposphere (Nicolet, 1975; Thrush, 1980; Bates and Jacob, 2019; Badia et al., 2021). The problem is that these family groupings, while intuitive and comforting, do not accurately produce the correct times scales or patterns of perturbations to the chemical system. We show later that the O_X family is not one of the inherent chemical mode patterns of the troposphere, and has the wrong timescales.

The tropospheric chemistry community has for the most part settled on diagnosing production and loss of tropospheric O_3 in the global models from the major rates for the O_X budget, e.g., from Table 4.12 in the 2001 IPCC assessment (Prather et al., 2001) to Table 6.3 in the 2021 assessment (Szopa et al., 2021)..

$$POx = k_1(T)\,[HO_2]\,[NO] + k_2(T)\,[RO_2]\,[NO] \quad (\textit{sometimes} + 2 \times J_{O2}\,[O_2]) \qquad (3)$$

$$LOx = k_3(T)\,[O(^1D)]\,[H_2O] + k_4(T)\,[O_3]\,[HO_2] + k_5\,[O_3]\,[OH] \qquad (4)$$

For the global troposphere, the history of major model intercomparison projects (MIPs) have reported POx and LOx in the range of 3500-5000 Tg-O_3 yr^{-1} with the balance of the budget made up of a source from stratosphere-troposphere exchange (400-600 Tg-O_3 yr^{-1}) and a sink to surface deposition (800-1200 Tg-O_3 yr^{-1}) (Prather et al., 2001; Stevenson et al., 2013, Young et al., 2018; Archibald et al., 2020; Griffiths et al., 2021; Szopa et al., 2021). These diagnostics reflect the major rates affecting O_3; they are now standard diagnostics for current chemistry models; and they have served as excellent diagnostics for understanding consistency and differences in the model calculated O_3.

The extensive use of PO_X and LO_X has created two problems. First, everyone has known that the true O_3 chemical tendency (dO_3/dt, Equation 1) is not exactly equal to PO_X–LO_X. Recently, the Archibald et al. (2020) study of tropospheric O_3 trends made a substantial effort to include the dO_3/dt budget term in analysing the four models that reported it, finding that it provided "a cleaner … account of the tendency of ozone" due to chemical processes. Hopefully, this effort will continue in future MIPs.

The second major problem with the O_X terms is the assumption that the O_3 chemical tendency equation can be written as at

$$d[O_3]/dt = +POx - fO3_{chem}\,[O_3] \qquad (5)$$

where the production PO_X is constant, independent of [O_3], and the loss frequency is calculated simply from LO_X,

$$fO3_{chem}^{LOX} = LOx\ /\ [O_3] \qquad (6)$$

This approach is popular and persistent because it puts O_3 in a parallel framework with other trace gases where production is due to sources that are independent of the species concentration and where loss is linearly proportional to the species concentration.

Follows and Austin (1992) with a 2D model and Roelofs and Lelieveld (1997) with a 3D model developed the approach of using the tagged tracer O3S in order to follow stratospheric O_3 entering the troposphere through stratosphere-troposphere exchange (STE). Using their photochemical box model, Follows and Austin (their Figure 10) followed the decay of an O_3 perturbation using full chemistry as is done here with a 3D model, but they reverted to using the simplified and inaccurate linear assumptions about LO_X (their Equation 11). This methodology continues in multi-model assessments of O_3 and climate change, such as Williams et al. (2019) and Abalos et al. (2020). Wild et al. (2003) used this O3S method but recognized that “this [approach] is not a correct linearization of the impact of an added flux of

stratospheric ozone," yet we have all continued using this approach for the last two decades. The loss frequency for O_3 should be derived from a linearization of the chemical tendency

$$fO3_{chem}^{TRUE} = d[-dO_3/dt] / d[O_3] \quad (7)$$

but 3D models are not prepared to do chemical linearizations every time step. Using the ATom-1 observations, Prather et al. (2023, Figure 68) showed that LO_X is not precisely linear in $[O_3]$, and more importantly that PO_X is not constant but decreases with increasing $[O_3]$. Hence, $fO3_{chem}^{TRUE}$ is 20-40% larger than $fO3_{chem}^{LOX}$, and thus currently modeled O3S values are too large. From the limited coverage of ATom observations we cannot derive a global pattern of $fO3_{chem}^{TRUE}$, but here we can calculate hemispheric mean values from the decay of O_3 perturbations.

2.2. The control run

The baseline for this study is a UCI CTM 5-year control run (CTRL) for years 2000 through 2004 that includes stratospheric-plus-tropospheric gas-phase chemistry with typical emissions and boundary conditions for years 2000 through 2004 (see Tang and Prather, 2012; Holmes et al., 2013; 2014). The CTM is driven by prescribed meteorology from the European Centre for Medium-Range Weather Forecasts (ECMWF) Integrated Forecast System (IFS, Cycle 38r1). Use of historical, specified meteorological fields for 1 Jan 2000 through 31 Dec 2004 means that any chemical perturbation can be tracked accurately to within the relative precision of the non-linear chemical solver, about 10^{-5}. With a chemistry-climate model (CCM), these experiments would require a number of ensembles to average the perturbations over climate variability, but here a single perturbation and control simulation are adequate. A summary of the UCI CTM chemistry and conditions for the CTRL run are given in the Appendix **Tables A1-A3**. A summary of the tropospheric O_3 budget (**Table 1**) has the UCI CTM falling within the range of models tabulated in recent MIPs (Young et al., 2018; Archibald et al., 2020; Griffiths et al., 2021).

For this study it is essential to be able to separate the troposphere from stratosphere, and thus we use instantaneous 3D fields of O_3 and e90, our artificial tracer of tropospheric air (Prather et al., 2011). The e90 tracer has a constant rate of decay (90 days) and is emitted uniformly over the globe at a rate to generate an average abundance of 100 ppb (nmol/mol). In this version q75 of our CTM, e90 = 90 ppb coincides with the WMO tropopause and is used categorize each grid cell as either tropospheric or stratospheric. Monthly averages of O_3 and e90, or even WMO tropopauses, smear across the synoptic variability of the tropopause, causing systematic errors in diagnosing tropospheric O_3. We compromise on continuity versus data volume by using 73 snapshots per year (every 5 days) that record the 3D mass fields of O_3, e90, and dry-air in each cell. The zonal-mean altitude-by-latitude color maps of CTRL stratospheric and tropospheric O_3 are shown in **Figure 1** and **Figures A1-A2**. Results here average over 18 snapshots in the 90 days of northern summer (JJA) over the five years and are typical of other models and observations. The seasonal and zonal average for stratospheric O_3 includes only stratospheric cells, so that if at least one of the 320 longitude cells over the 18 snapshots is stratospheric a non-blank value is shown for that pixel. Thus, the same pixel can be included in both figures.

The annual variability in global mean stratospheric and tropospheric O_3 in Dobson units (DU) is shown in **Figure 2** and **Figure A3**. Over the 5-year CTRL run, the tropospheric mean column varies from about 28 DU (Feb) to a sharp peak of about 34 DU (Oct) occurring within a 10-day period (1 DU global = 10.9 Tg-O_3). These values are consistent with the observed columns (about 30 DU) and seasonal cycle (minimum in DJF) found by Ziemke et al. (2006; 2012). This synoptic 5-day variability as well as the interannual

changes are driven by the meteorological changes (H_2O, T, transport) since emissions vary only monthly and are recycled each year. Likewise, the lower boundary conditions for CH_4, H_2, and N_2O are constant. Lightning NO emissions are tied to convection but vary at most by 6% from year to year. In contrast, the stratospheric column varies smoothly, from 270 DU (~Sep-Oct) to about 290 DU (Mar). This stratospheric O_3 annual cycle along with the longer-term quasi-biennial variability matches latitudinal patterns seen in satellite observations (Figure 9 of Ruiz and Prather, 2022). Looking at the synoptic variability, one might infer that the sharp tropospheric O_3 peak in Oct is carried into the stratospheric O_3 column and thus long-term tropospheric O_3 trends and variability will alter the stratospheric O_3 column.

2.3. Simulating direct O_3 emissions

Trying to diagnose the budget lifetime and timescales of tropospheric O_3 perturbations from a combination of reaction rates or their derivatives with respect to O_3 is an unrewarding task. So instead we propose a CTM model experiment in which we directly emit O_3 at a fixed rate (100 Tg-O_3 yr^{-1}) for several years and follow the increased burden of O_3. This perturbation allows all of tropospheric chemistry to change in response and gives us the perturbation lifetime for that specific pattern of emissions. Then, we cut emissions and watch the decay time of the chemical modes so we can diagnose the timescale of O_3 perturbations. Remembering the eigenvalue decomposition of the system (Prather, 2007), we expect the lifetime (i.e., burden in this case) to depend on the location-timing of emissions, but the timescale of each chemical mode will be a property of the CTRL atmosphere and independent of the emission pattern. The amplitude of each mode, however, will depend on the emission pattern.

The direct O_3 emissions are added as a perturbation to a control run (CTRL) simulation and are designated eO3x, where 'x' designates the specific case, see **Table 1**. Three different types of direct O_3 emissions are explored: eO3avi, 100 Tg-O_3 emitted per year using the same pattern as aviation NOx; eO3srf, 100 Tg-O_3 yr^{-1} as near-surface emissions from east Asia (34°N-40°N; 110°E-140°E), consistent with the net production of 130 Gg per day found for East Asia (Wild and Prather, 2006); and eO3ste1, 100 Tg-O_3 yr^{-1} centred on the subtropical jets, meant to simulate a fraction of the net influx of stratospheric O_3 (as modeled in Prather et al. 2011; Ruiz and Prather, 2022). The first eO3ste1 experiment resulted in large amounts of O_3 accumulating in the stratosphere, which complicated the calculation of O_3 lifetime. Thus, we relocated the emissions and reran this experiment as eO3ste2, see the latitude shift of emissions in Table 1. To compare the O_3 perturbation from direct emissions versus the secondary O_3 produced from aviation NOx, we added experiment eNOavi, for which the aviation NOx emissions (0.85 Tg-N y^{-1}) are doubled. See **Table 1** for details of each experiment.

The eO3x experiments are run for 4 years (2000.0 to 2004.0). For eO3avi, eO3srf, and eO3ste1, we run separate 6-month decay experiments, cutting the direct O_3 emissions at 2003.5 (1 Jul) and 2004.0 (1 Jan). **Figure 2** shows the resulting perturbations in DU for eO3avi tropospheric (blue) and stratospheric (red) O_3. **Figure A4** shows parallel results for eO3srf and eO3ste1. Our estimated lifetime for the eO3avi O_3 perturbation, 20 days, is similar to most previous values for total tropospheric lifetime (e.g., Badia et al., 2021). Thus, the O_3 lifetime is sub-seasonal, <1 month; and O_3 perturbations will not mix between hemispheres and will respond to the seasonal variations in photochemical activity. With a fixed boundary condition on CH_4, the longest chemical response will likely be CO (~2 months) and thus the spin-up and decay times as seen are at most 6 months. Statistics on the O_3 perturbations (**Table 1**) use only the 2nd through 4th year.

Several experiments (eO3avi, eO3ste1, eO3ste2) result in a minor fraction of O_3 emissions occurring in the stratosphere. We tried to minimize direct stratospheric emissions but did not rewrite the CTM code to turn on/off emissions at every time step for each grid cell based on the e90 tropopause definition. In our

studies, these direct stratospheric emissions occur well below 100 hPa and thus accumulate mainly in the lowermost extra-tropical stratosphere (LMS). Ozone chemistry in the LMS, except for the Antarctic ozone hole, is slow, and transport into the troposphere occurs mostly within a year. Thus, direct O_3 emissions into the LMS tend to accumulate until they are transported into the troposphere via stratosphere-troposphere exchange (STE), and thus the 100 Tg-O_3 yr^{-1} emissions in eO3avi, eO3ste1, and eO3ste2 can be treated tropospheric emissions albeit with some seasonal delay from the STE flux.

3. Results

The lifetimes and patterns of the O_3 perturbations are distinct to each type of emission. The perturbations are all responding to tropospheric chemistry that is damping the perturbations at different locations and seasons according the photochemical reactivity. For a quick survey of the profiles and variability of production and loss of O_X over the Pacific basin from a multi-model comparison, see Figure 3bc of Prather et al. (2017) and from the NASA Atmospheric Tomography Mission (ATom) observations, see Figures 6-7 of Prather et al. (2023). From the observations, there is large high-frequency variability on the scale of a model grid; and from the models, there are large differences in mean profiles.

3.1. Spatial pattern of O_3 perturbations

The zonal mean (latitude by altitude) pattern of O_3 absolute perturbations (ppb) are shown in **Figure 3** for JJA, showing eO3avi (left) and eO3srf (right) separated by stratosphere (top) and troposphere (bottom). Parallel plots are shown for all four seasons and all five experiments in **Figures A5-A9**. For these plots, the stratospheric and tropospheric color bars are same (0 to 12 ppb); plotting relative differences would greatly reduce the intensity of the stratospheric perturbation.

Aviation emissions, eO3avi, include a number of high-latitude, stratospheric flight routes below 12 km altitude (lowest horizontal black line in **Figure 3**). These emissions are seen clearly by the build-up of a 10-12 ppb perturbation from 8 to 12 km in the stratosphere. There is some transport of excess O_3 to higher altitudes in the tropics along isentropic surfaces, but this does not get above 16 km altitude and stays in the LMS. Chemical loss of the excess O_3 is more rapid in the troposphere as is vertical mixing, and the peak build-up in northern mid-latitude flight lanes (8-12 km) is less, about 6 ppb. In northern summer, the loss of excess O_3 is rapid in the lower troposphere, and the excess O_3 barely reaches the surface with perturbations of ~1 ppb. In northern winter (DJF, **Figure A5**) with much slower chemistry, surface perturbations are much greater, ~3 ppb. Emissions in the southern mid-latitudes are much smaller and barely show up in the stratosphere (~1 ppb) and not in the troposphere with this color scale.

For surface emissions (eO3srf), the peak zonal mean perturbations are 4-6 ppb in the latitude-altitude region of emissions (black box in **Figure 3**). These emissions are mixed upward to the tropopause at levels of ~2 ppb but fall off rapidly in the subtropics and at higher latitudes, again because of the rapid loss of excess O_3 in the northern summer lower troposphere. It is interesting that summertime O_3 pollution from the northern mid-latitudes is not expected to reach the polar lower troposphere, but during the other three seasons (SON, DJF, MAM) the surface emissions in eO3srf collect at moderately high levels (~3 ppb) throughout the mid-latitude and polar troposphere (**Figure A7**). eO3srf has no direct stratospheric emissions, and so the LMS enhancement of ~2 ppb is driven by the tropospheric increases.

The O_3 perturbations patterns for eO3ste1 and eO3ste2 (**Figures A8-A9**) are quite different in the stratosphere because of eO3ste1's much greater fraction of emissions directly into the stratosphere; however, their tropospheric patterns are quite similar because the net tropospheric emissions are almost identical as explained above. Focusing on the latitude-altitude patterns for eO3ste2 (**Figure A9**), it appears to be difficult in any season for the STE O_3 flux to reach the surface in mid-latitudes. The

simplest explanation is that this flux mostly enters the troposphere about the tropical jet stream and is transported first along isentropic surfaces into the subtropics where chemical loss of O_3 remains high year-round.

3.2. Variability in O_3 columns

The O_3 column (DU) in these experiments is split into stratosphere and troposphere using the 5-day snapshots. The latitude-by-day plot of these two columns for CTRL year 2003 (**Figure A10**) shows the variability of this high-frequency sampling: the Antarctic ozone hole is clear as are the Arctic wintertime vortex breakdowns (Feb-Apr), which bring high O_3 columns (>450 DU) to the pole. In our experiments, most of the perturbations to column O_3 are dominated by the troposphere except for eO3ste1. Zonal mean O_3 column perturbations versus latitude are shown for all five experiments in **Figures A11-A15** from years 2000 through 2003. The spin up of the perturbation in the first half of year 2000 is notable in all experiments. The STE experiments eO3ste1 and eO3ste2 show minimal seasonal variability and clear hemispheric symmetry. The southern hemisphere has a slightly larger build-up, probably because the northern hemisphere has greater pollution and more rapid O_3 loss. The surface emissions eO3srf shows a clear peak column perturbation of ~2 DU over the source region near 38°N, with equally large wintertime maxima extending to 90°N. The direct aviation emissions eO3avi shows a similar pattern to eO3srf but with less variability since the source is more diffuse. Aviation NOx emissions eNOavi have a distinct seasonality because of the photochemical variability in the production of O_3 from the NOx perturbation. eNOavi peaks in the summer and fall (as opposed to winter in eO3avi) with the maximum following the solar declination from 30°N in winter to 45°N in summer. Clearly eO3avi, even if scaled, is not a good surrogate for the impact of aviation on O_3.

3.3. Burdens and lifetimes

The burden of excess tropospheric O_3 in Tg divided by the 100 Tg-O_3 yr^{-1} emissions defines the perturbation lifetime as given in **Table 1** and shown in **Figure 4**. See also **Figure A16** for the total excess burden and **Figure A17** for separate plots of each experiment comparing tropospheric, stratospheric and total burden. For experiment eNOavi, which does not have direct O_3 emissions, we cannot define a lifetime for the O_3 perturbation, so ignore the right axis. Both STE experiments (eO3ste1 and eO3ste2) are surprisingly similar in terms of tropospheric burden; both have similar lifetimes (~25 days); and both show little seasonality. Aviation direct O_3 (eO3avi) is the next largest burden, but it shows large seasonality, accumulating more in northern winter. The surface O_3 (eO3srf) has the smallest burden and the largest seasonality in lifetime, from 6 days in summer to 21 days in winter. This sequence in lifetimes reflects the distance from emissions to photochemical sink, including surface deposition in these calculations. The sink in this case is the lower troposphere in the tropics or the summertime mid-latitudes (see Figures 7 and 11 of Prather et al., 2023).

Excess O_3 peaks in January for eO3avi and eO3srf because there is a lower loss rate in NH winter. Such seasonality is unrealistic for typical pollution sources such as urban or aviation because the production of O_3 also drops substantially in winter. For eO3avi, the max:min (winter:summer) ratio of excess burden is 1.63, while for eNOavi, it is 1.22. The eNOavi excess burden is much less seasonal than that of eO3avi because the excess O_3 produced from aviation NOx scales with O_3 loss and overall photochemical activity. We expect similar results for urban pollution (eO3srf) but could not define a simple emission scenario to test this.

3.4. Chemical modes and timescales

The steady-state patterns of O_3 perturbations are unique to each emission pattern (e.g. **Figures 3, A5-A9**). The eO3avi/srf/ste1 zonal mean latitude-by-altitude patterns for 1 July 2003 and 1 January 2004 are shown in **Figure A19**; and these are the initial patterns just before our decay experiment in which we stop emissions. The subsequent decay of the NH tropospheric burden of excess O_3 is shown in **Figure 5** (top), with the SH burden decay shown in **Figure A18**. All excess burdens are scaled to a value of 1 at the start of decay, and the y-axis is logarithmic so that constant decay rates are straight lines. Constant decay lines of 10, 20, 30 and 40 days (left to right) are shown to guide the eye. In NH summer, the burdens start to decay with e-fold timescales between 10 and 20 days; while in winter the initial rate is much slower, 30-40 days. In NH summer, rates slow down (become flatter) after two months as we enter the fall; while in winter, they speed up (become steeper) as we enter the spring.

The surface emission patterns (eO3srf) start to decay more rapidly than the upper tropospheric patterns (eO3avi and eO3ste1) because more excess O_3 is near the surface where O_3 loss is more rapid from both chemistry and surface deposition. After a month or so, they tend to follow more parallel decay rates because the remaining O_3 is in a primary chemical mode with largest perturbations in the northern mid-latitude upper troposphere. We can identify this primary O_3 mode, as the zonal mean altitude-by-latitude color maps in **Figures 5** (bottom) and **A20**. To calculate these modes, we drop the first month to allow short-term chemical modes to decay. These short-term modes will be primarily related to rapid transport of O_3 from the emission zone to neighboring regions. We then take the perturbation for days 30, 35, …, and 85 (months 2-3), scale each day's perturbation to a NH tropospheric O_3 perturbation of 5 Tg, and then average them. The patterns of excess O_3 for eO3avi, eO3srf, and eO3ste1 are remarkably similar and indicate that we have found the primary O_3 mode, at least for the mid-latitudes. The timescales here of 10-40 days are is similar to a range of intra-hemispheric transport and mixing scales, and there may be several overlapping modes in each hemisphere. We do not expect the emergence of a clean, single global mode as we found in similar experiments with N_2O and CH_4 (Hsu and Prather, 2010; Prather and Hsu, 2010).

3.5. Perturbations across other species

The emission-driven O_3 increases perturb all of tropospheric chemistry. In **Table 2** we present a brief summary of the relative changes in the northern extra-tropics for key species and rates from eO3avi on 1 July 2003. We find that most perturbations maximize in the upper troposphere (200-600 hPa) vs the lower troposphere (600-1000 hPa): +5.6% vs. +3.5% for O_3 and -3.5% vs. -3.1% for NOx. The NO depletion is larger than that of NOx and similar in both parts of the troposphere, about -5%, but still, NO_2 is depleted. The OH and HO_2 changes are more complex with HO_2 increasing and OH decreasing aloft, while both increasing near the surface. From the OH increase in the lower troposphere, the global loss rate of CH_4 and CO to OH reactions increases, but by $\leq 0.1\%$.

The full latitude-by-altitude eO3avi patterns in % change for O_3, NO, NO_2, HNO_3, PAN, CO, C_2H_6, C_3H_8, HOOH, CH_3OOH, and HCHO are shown in **Figure A21**. The patterns here are consistent with the location of eO3avi emissions, but are also related to the O_3 primary chemical mode (**Figure A20**). The O_3 increase is large (3-5%) and extensive (35°N-90°N, 6-11 km), and NOx is reduced (1-3%) over a similar domain. The OH radicals (not shown) are reduced, and thus the VOCs (CO, C_2H_6, Alkane) increase by a fraction of 1%. The reduction in NOx drives increased peroxides (H_2O_2, CH_3OOH, PAN). Formaldehyde (HCHO) shows small, plus-minus changes indicating that overall production of methyl radicals, a primary source of HCHO, is not changed. These patterns are probably similar for STE fluxes, but may not apply to surface O_3 fluxes.

The general concept that NO_2 is part of the O_X family and that an increase in O_3 would be accompanied by an increase in NO_2 is not borne out with a perturbation to O_3 in a full chemistry model

4. Discussion and implications

4.1. Lifetimes

With these direct O_3 emission experiments, we are calculating a 'perturbation lifetime', i.e., the excess burden of tropospheric O_3 divided by its emission rate. Lifetimes calculated here with the UCI CTM include chemical loss and surface (dry) deposition. Lifetimes vary seasonally, but fortunately with values <30 days, a steady state is reached for each season. This steady-state condition is critical because then the product of the lifetime times the 3D steady-state pattern are equivalent to the integral of impacts over the decay of a single-pulse emission, see theorem in Prather (2007). Calculation of perturbation lifetimes for tropospheric O_3 are rare (e.g., Figure 11 of Hsu and Prather (2009) estimates the lifetime from the slope of the tropospheric O_3 burden vs. the STE flux from a CTM experiment and gets 27-34 days). Most of the 'lifetimes' we have discussed here are actually the inverse of the tropospheric mean loss frequency for O_X. Such lifetimes have no essential link to the chemical modes and timescales of the tropospheric O_3 system, yet their values are similar to the perturbation lifetimes. Is that fortuitous? or is there some underlying physics relating them? There are clearly problems with the inverse-loss lifetimes: they are singular in value; and they do not readily include the chemical feedbacks of O_3 on its production and loss. As a model metric for tropospheric O_3 that has followed the development of CCMs and CTMs for over two decades, the lifetime derived from LO_X remains an incredibly valuable diagnostic and its use should be continued with the same consistent definition (equation 4), but it should not be confused with a true lifetime or used for timescales.

4.2. STE and tagged tracers

An obvious application of this work is a more accurate attribution of the role of STE on tropospheric O_3 and surface air quality. If we scale our eO3ste experiments to an observation-based STE flux of about 400 Tg-O_3 yr^{-1} (Murphy and Fahey, 1994; McLinden et al., 2000; Olsen et al., 2001; Ruiz and Prather, 2022), then a lifetime of 24 days scales to 26 TgO_3 or about 8% of the tropospheric burden. Even if we use the multi-model LO_X-based lifetime range of 24-32 days (Griffiths et al., 2021), and correct them for O_3 chemical feedbacks, we get similar results. So, what is wrong with the tagged tracer O3S that measures stratospheric influence at about 40%? (Roelofs and Lelieveld, 1997; Williams et al., 2019; Abalos et al., 2020). The O3S calculations use local values of $fO3_{chem}{}^{LOX}$ as the loss frequency, and we know that this underestimates the loss by 20-40% because it fails to account for O_3 chemical feedbacks, but this is only a small fraction of the difference. This factor-of-5 difference in stratospheric influence could be seen as simply definitional, but there are important implications for understanding future O_3. A number of model studies have estimated STE flux increases of up to 150 Tg-O_3 yr^{-1} over the 21st century (Hegglin and Shepherd, 2009; Meul et al., 2018; Abalos et al., 2020; Wang and Fu, 2023). These models then exaggerate the resulting increase in tropospheric O_3 attributable to this STE flux as being 15% (50 Tg-O_3); whereas we would calculate that increase to be 3% (10 Tg-O_3). Fortunately, the models are calculating the 'correct' overall tropospheric O_3 change for their CCM under scenario RCP-8.5 because the tagged tracer O3S does not change the chemistry of O_3. Nevertheless, the attribution to the increased STE O_3 flux is misleading for policy use.

When we then try to attribute the O_3 changes to specific factors using a tagged O_3 tracer, we err. The fundamental problem is that O_3 and O3S are interchangeable in terms of the chemistry and because O_3 is a dominant species, a perturbation to O3S should be felt across all of tropospheric chemistry. Effectively, it increases the loss of the baseline O_3 which is not included with the tagged tracer experiment. A parallel

case can be easily seen with CH_4. Assume that CH_4. has global lifetime of 9 yr and a perturbation lifetime of 12 yr. We add a small amount (1 Tg) of tagged CH_4 from riverine sources, CH4R. The perturbation is small (0.02%) and so the OH lifetime perturbation is also small (~0.006%). The tagged CH4R will thus decay with a 9 yr e-fold; however, we know that, and calculate that the overall 1 Tg perturbation to CH_4 decays with a 12 yr e-fold. We can reconcile this conundrum by realizing that the perturbation caused by CH4R is small but it applies to the entire CH_4 system, and thus it is increases in the non-tagged CH_4 that makes the perturbation decay with a 12 yr e-fold. For O3 and O3S, the case is parallel but the chemical feedbacks are opposite: increased O_3 leads to more rapid O_3 loss and thus O3S causes more rapid loss of total O_3 and its effective perturbation should decay more rapidly than the linear loss frequency used in O3S experiments. The decay of the influence of STE is accurately modeled with a perturbation experiment as here.

4.3. Other chemical perturbations

Our experiments with 100 Tg annual emissions of tropospheric O_3 increase CH_4 loss via OH by about 0.08% (eO3avi/srf) and 0.10% (eO3ste1/ste2). eO3avi/srf are slightly less effective because the impacts are mostly in NH mid-latitudes, while most of the CH_4 is lost in the tropics favouring the STE fluxes of eO3ste1/ste2. Aviation NOx emissions that lead to a similar increase in O_3 have a much larger impact on CH_4 loss, +1.24%, because the NOx shifts HO_2 into OH. Thus, we can attribute aviation's impact on tropospheric chemistry overall to the direct impact of NOx emissions rather than to the secondary build-up of an O_3 perturbation, although the latter is a major component of aviation's climatic impact (Lee et al., 2020).

Comparing the build-up of O_3 as a secondary pollutant from aviation NOx with that of the direct emissions, we find that the extra 0.85 Tg-N yr^{-1} from eNOavi produces 4.82 Tg excess O_3 at steady state, which is 91% of eO3avi's perturbation and thus equivalent to 91 Tg-O_3 yr^{-1}. Converting to moles, we calculate an annual-mean ozone production efficiency (OPE) of 31 moles of O_3 produced per mole of NO emitted by aircraft, with a wintertime low of 24 on Jan 7 to a summertime high of 40 on Jul 1. This OPE estimate is only approximate because we use the perturbation lifetime from eO3avi to scale the eNOavi O_3 perturbation into a flux (Tg yr^{-1}). These values are consistent with OPE values for low-NOx conditions in the free troposphere found in a variety of locations (Kleinman et al., 2002; Wild and Prather, 2006; Mazucca et al., 2016), and provide a novel way of calculating OPE. Nevertheless, the concept of an OPE is mainly heuristic, the impact of aviation can only be assessed from the excess O_3 calculated with an eNOavi experiment.

4.4. Odd oxygen and family chemistry

The long-standing effort of the atmospheric chemistry community to group species into families has been productive, but for tropospheric O_3 this has reached new levels of complexity (Bates and Jacob, 2019; Badia et al., 2021; Archibald et al., 2020). A major goal in defining an O_X family is to describe a co-varying set of species (like an eigenvector or chemical mode) whose net chemical reactions in and out can be used to estimate a loss frequency (like an eigenvalue). Yet to date, these efforts in abstracting tropospheric chemistry have not been able to address the nature of the chemical feedbacks. More complex definitions of odd oxygen have led to large increases in its lifetime that are simply not found in O_3 perturbation experiments. Further, a staple in the O_X family has always been NO_2, but we find that tropospheric O_3 perturbations are linked with decreases in NO_2, so that the family definition does not represent a fundamental chemical mode of the troposphere. This results was somewhat surprising and disappointing because $O_X = O_3 + O$ is one of the chemical modes for Chapman chemistry in the stratosphere.

4.5. Remaining issues

How robust are the results here? We suspect they are within the 20% range that describes most of the differences across models (e.g., Stevenson et al., 2013; Young et al., 2018; Griffiths et al., 2021), including the UCI CTM. The results here do not depend on cancelling effects, and the chemical perturbations and feedbacks driven by O_3 changes are straightforward and easy to assess.

Seasonality is a core element of the tropospheric O_3 budget, both production and loss, as found in the seasonality of the four Atom deployments (Prather et al., 2023). Fortunately, the O_3 timescales are much less than one season, a near steady state is reached within 1-2 months, and so one must consider separately the seasonal cycles in O_3 production or STE flux. For example, the wintertime accumulation of direct surface emissions (eO3srf) fills the NH extratropical troposphere because O_3 loss is suppressed during NH winter. That pattern of excess O_3 is likely correct but the magnitude is exaggerated because surface production of secondary O_3 pollution drops off outside of JJA. In the case of aviation, we directly diagnose a reduction in wintertime O_3 production with experiment eNOavi, finding the accumulation of excess O_3 to be seasonally flat. Experiments like these, with simplified direct emissions, can be used in global chemistry models to diagnose the seasonal response of tropospheric O_3 perturbations to combined chemistry and transport. Direct perturbation experiments, either emission or pulse, also avoid the foibles of tagged tracers with incorrectly linearized chemistry, and they provide a more accurate assessment that includes full chemical feedbacks.

Author Contributions

MJP designed, drafted and revised the paper; XZ designed and performed the CTM calculations; MJP & XZ analyzed the CTM data and prepared the figures and tables.

Acknowledgments

We thank P. Griffiths and J. Keeble for helpful discussions during the formulation of this research, particularly for the efforts to design the next MIP focusing on atmospheric chemistry and the short-lived climate forcers.

Funding Information

Research at UCI was supported by grants NSF AGS-2135749 and NASA 80NSSC21K1454.

Competing interests

The authors declare that they have no competing interests.

Supplemental material

Supplemental material as figures and tables are included as a pdf file.

Data Accessibility

The high-frequency 3-D datasets calculated with the UCI CTM and used in this study are provided in a Dryad archive (Prather, 2024). The Matlab scripts and a full set of .eps figures are provided in the parallel Zenodo archive.

Figures & Tables

Table 1. CTM experiments

run	emissions	notes
CTRL	Control run	
eO3avi (EO3A)	+100 Tg-O_3 yr^{-1}	Aviation: NO emission pattern, RCP6.0 y2000
eNOavi (EO3B)	+0.85 Tg-N yr^{-1} (2xAviation NOx)	Aviation: NO emission pattern, RCP6.0 y2000
eO3srf (EO3S)	+100 Tg-O_3 yr^{-1}	Surface: 34°N–40°N; 110°E–140°E; 0–2 km
eO3ste1 (EO3T)	+100 Tg-O_3 yr^{-1}	STE: 25°S–35°S & 27°N–37°N; 11.0–12.2 km
eO3ste2 (EO3U)	+100 Tg-O_3 yr^{-1}	STE: 15°S–25°S & 15°N–25°N; 11.0–12.2 km

CTRL: O_3 budget	**P–O_3**	**L–O_3**	**P–L (O_3)**	**DD–O_3**	**Residual (STE)**	**L–O_X**	**mean loss frequency**
Tg-O_3 yr^{-1}	23,963	23,695	269	628	359	4,656	(23.8 days)$^{-1}$

	perturbation O_3 burden (Tg-O_3)		**perturbation O_3 lifetime (days)**
run	**troposphere**	**stratosphere**	**troposphere**
CTRL	345	3,045	na
eO3avi	5.32 (4.28 – 6.98)	1.66 (0.63 – 2.70)	19 (16 – 25)
eNOavi	4.82 (4.14 – 5.24)	0.34 (0.22 – 0.45)	not defined
eO3srf	3.46 (1.59 – 5.77)	0.16 (0.10 – 0.25)	13 (6 – 21)
eO3ste1	6.84 (6.35 – 7.49)	3.59 (2.51 – 4.73)	25 (23 – 27)
eO3ste2	6.44 (6.09 – 7.00)	0.98 (0.69 – 1.39)	24 (22 – 26)

Notes: All UCI CTM results are averaged over three years (2001-2003). The O_3 budget for CTRL is similar to other models for present day (1995-2004) in Table 1 of Griffiths et al. (2021) and Figure 3 of Young et al. (2018). Note that P (L) of O_3 are derived from the positive (negative) terms in Equation 1, so that P–L is the true d[O_3]/dt|chem of Archibald et al. (2020). L–O_X is taken from Equation 4 and can be directly compared with 'L' in these MIP tables. The mean loss frequency is calculated as the burden (345 Tg) divided by the sum of dry deposition (628 Tg yr^{-1}) plus L–O_X (4656 Tg yr^{-1}). Burden (Tg-O_3) and lifetime (days) for the eO3xxx experiments are shown as: mean (min – max). Perturbation lifetime assumes that effectively all emissions (100 Tg-O_3 yr^{-1}) are going into the troposphere, even if some originates in the stratosphere. Shorthand notation for files and some legends is shown in 'EO3X' format.

Table 2. Perturbation to key species as % in mass of CTRL for NH extra-tropics eO3avi on 1 July 2003

pressure range	O_3	HO_2	OH^a	NOx	NO
200–600 hPa	+5.6%	+1.3%	–0.3%	–3.5%	–4.8%
600–1000 hPa	+3.5%	+0.3%	+0.6%	–3.1%	–5.5%

Notes: Global tropospheric % change scaled by a factor of 4 to estimate the % change if all occurring in the northern extra-tropics (30°N-90°N) where most of the O_3 perturbation occurs. OH^a is weighted by CH_4 loss. The excess O_3 loss that balances emissions (8.8 Tg for the month of July 2003) is about equally split between upper and lower troposphere.

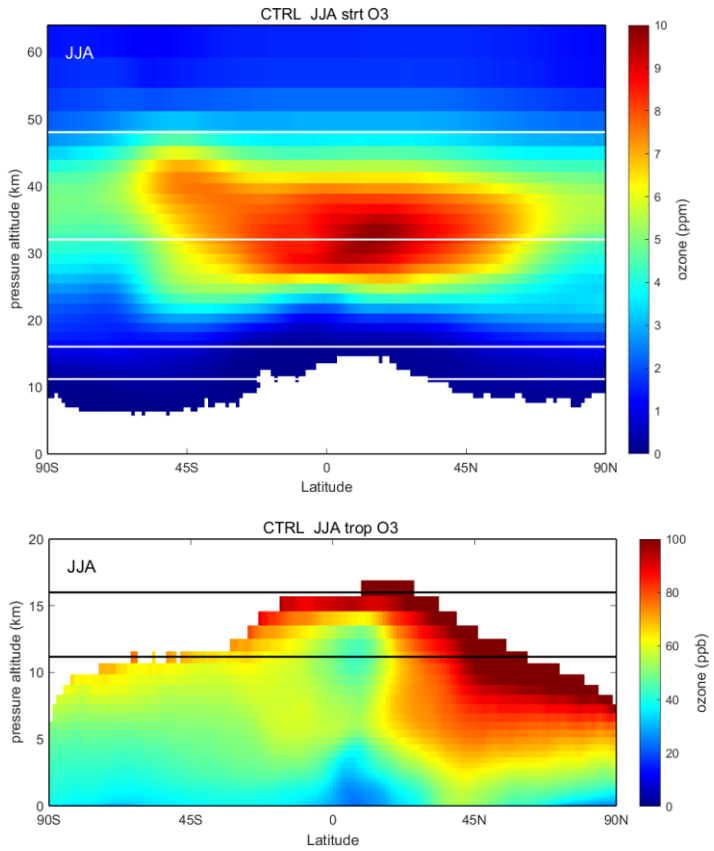

Figure 1. **Stratospheric and tropospheric zonal mean O_3 abundance** (ppm and ppb, respectively) averaged over June-July-August using 18 5-day snapshots from the CTRL run. Coordinates are latitude by pressure altitude z* = 16 km $\log_{10}(1/P(\text{bars}))$ and assume a surface pressure everywhere of 1 bar. Some pixels in this plot contain both stratospheric and tropospheric values because the pixel contained was both stratospheric and tropospheric air over the 18 snapshots and 320 longitude cells (e.g., stratospheric intrusions).

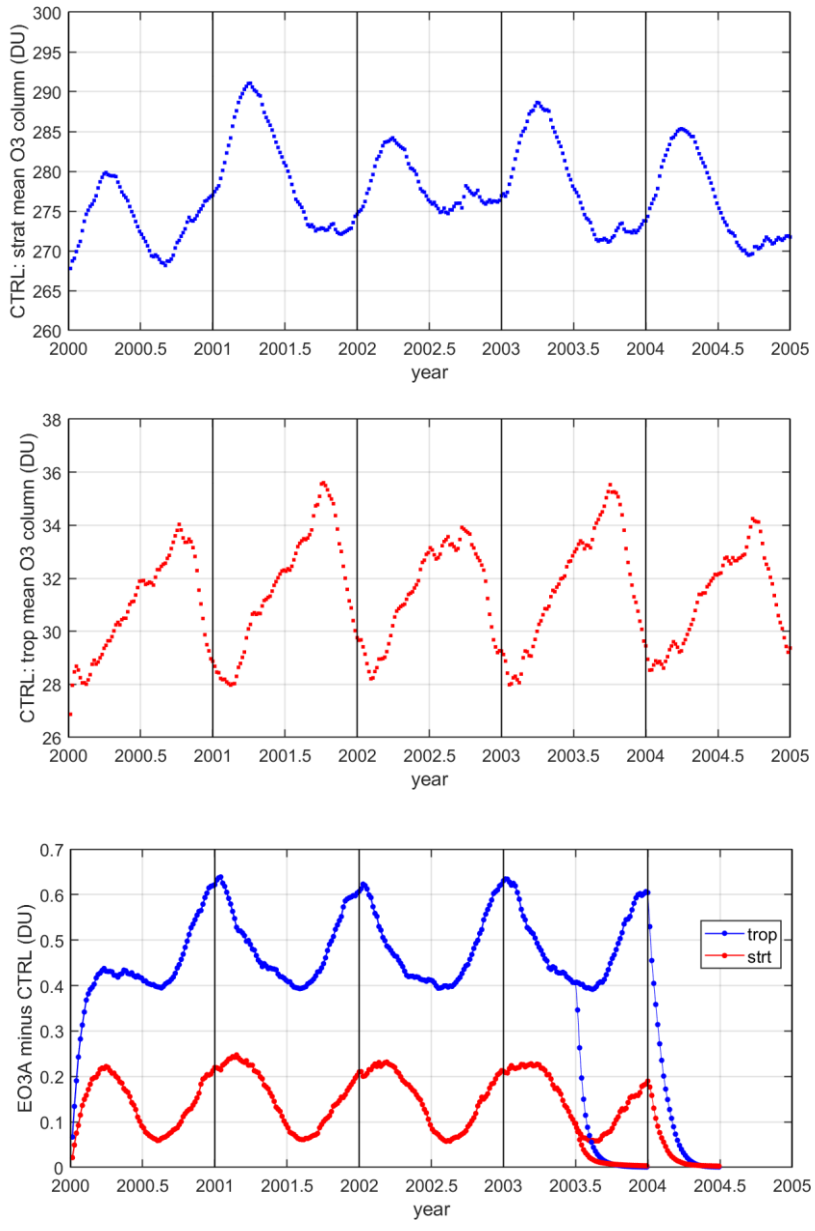

Figure 2. (top panels) Stratospheric and tropospheric mean O_3 columns (DU) from the CTRL run calculated from the 365 5-day snapshots over the five years, 2000 through 2004. (bottom panel) **Perturbation in the O_3 column (DU) for eO3avi (EO3A)**, separating troposphere (blue) from stratosphere (red). Also shown are the decay of the eO3avi perturbations after cessation of emissions on July 1 (2003.5) and Jan 1 (2004.0). In terms of global column, 1 DU = 10.9 Tg-O_3, and thus 100 Tg-O_3 yr^{-1} = 9.2 DU yr^{-1}, and a tropospheric column perturbation of 0.5 DU corresponds to a lifetime of 20 days.

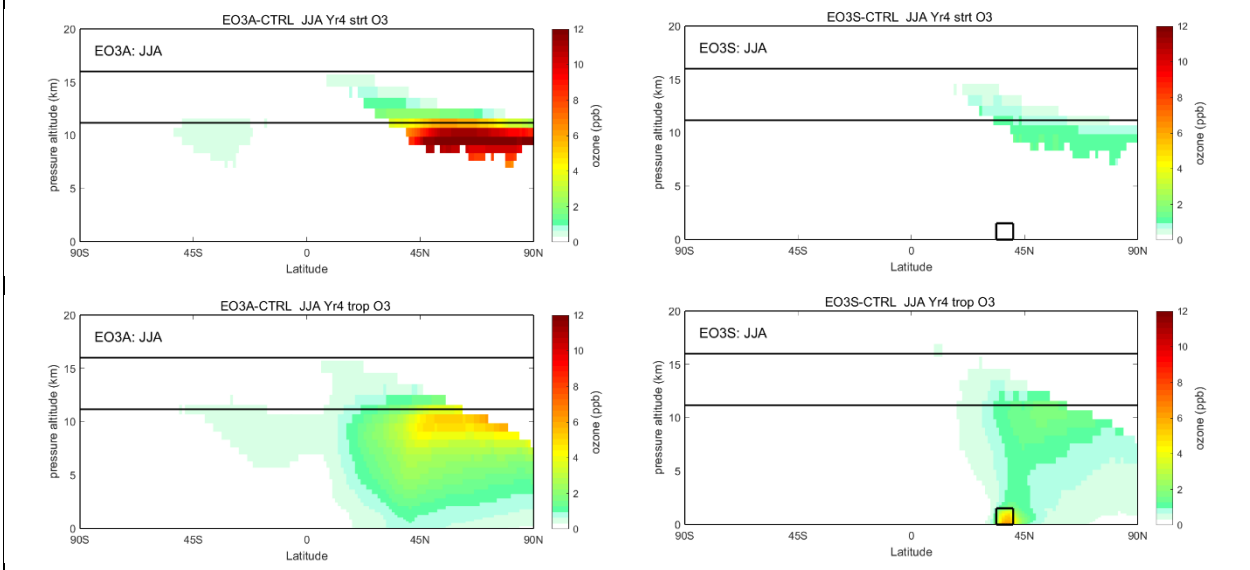

Figure 3. Perturbation to zonal mean O_3 abundance (ppb) in boreal summer (JJA) for eO3avi (EO3A, left panels) and eO3srf (EO3S, right panels), split into stratospheric (top panels) and tropospheric (bottom panels). For methodology, see Figure 1. Aviation emissions eO3avi occur mostly in the northern troposphere but reach into the stratosphere and southern hemisphere. Surface emissions eO3srf occur within the black square over a limited longitude range, see Table 1. Note that color bars have the same range on all plots.

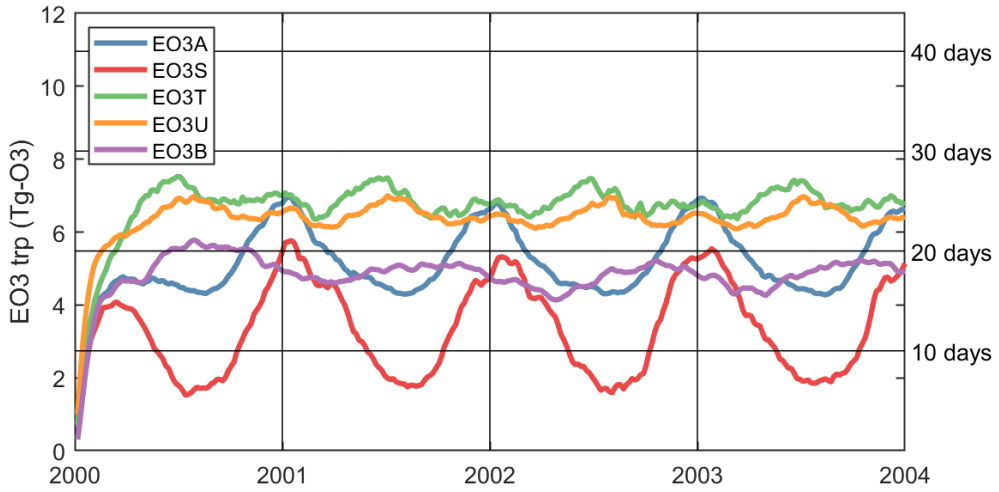

Figure 4. Tropospheric burden of excess O_3 (Tg) for the five experiments, showing 5-day intervals for years 2000 through 2003. The spin up in early 2000 is clearly visible. The lifetime scale (days, right axis) is calculated from the emission rate of 100 Tg-O_3 yr^{-1} for both tropospheric and total burden, and it does not apply to eNOavi. The legend notation is: EO3A = eO3avi; EO3S = eO3srf; EO3T = eO3ste1; EO3U = eO3ste2; EO3B = eNOavi.

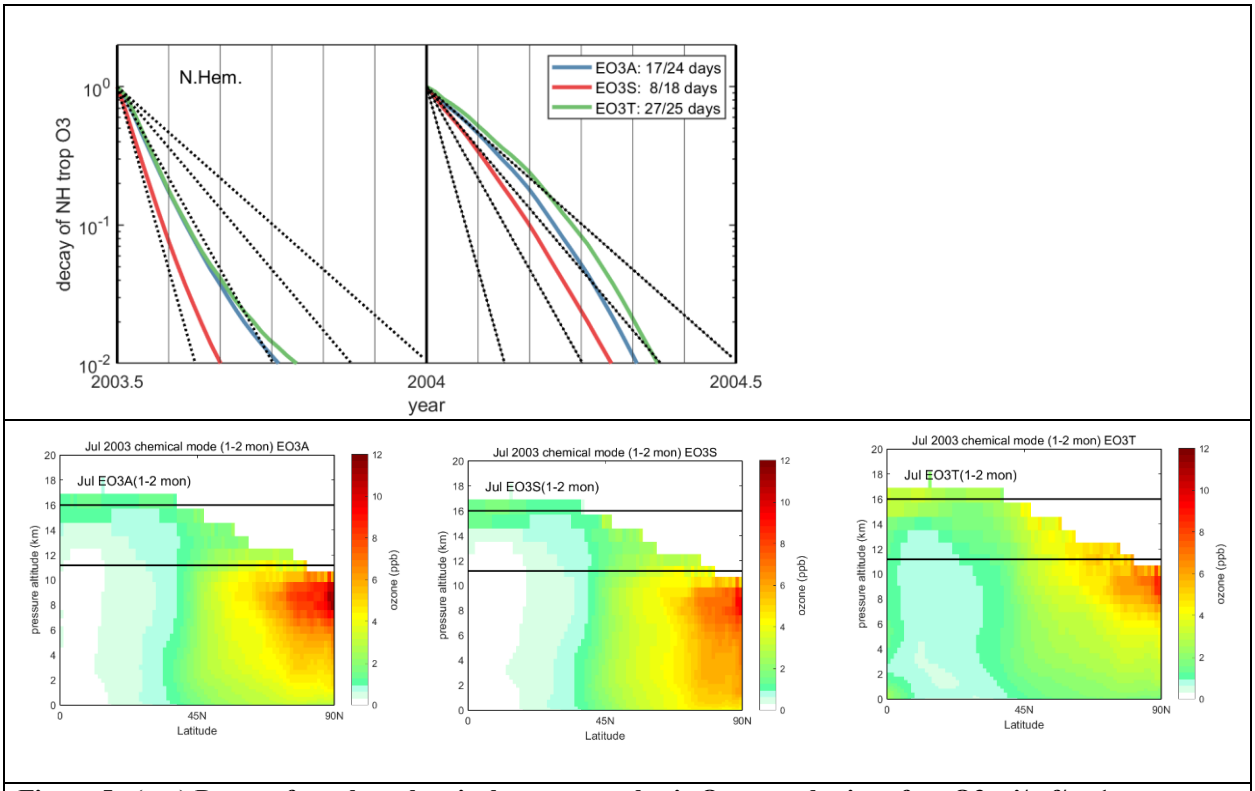

Figure 5. (top) Decay of northern hemisphere tropospheric O_3 perturbations for eO3avi/srf/ste1 (EO3A/S/T) rescaled to 1 at the time of cessation of emissions on July 1 (left) and January 1 (right). Dashed black lines are the same in both panels and show a constant decay of 10– (steepest), 20–, 30– and 40–day e–folds. The legend gives the min-to-max range in steady-state lifetime. Months are marked with vertical lines**. (bottom) Chemical mode patterns for the troposphere following decay of eO3avi/srf/ste1** starting at 1 Jul 2003. Modes are calculated from averaged NH patterns after 1–2 months decay (days 30–85). All perturbations are scaled to a total NH tropospheric O_3 perturbation of 5 Tg.

References

Abalos, M., Orbe, C., Kinnison, D. E., Plummer, D., Oman, L. D., Jöckel, P., Morgenstern, O., Garcia, R. R., Zeng, G., Stone, K. A., and Dameris, M. (2020) Future trends in stratosphere-to-troposphere transport in CCMI models, Atmos. Chem. Phys., 20, 6883–6901, doi:10.5194/acp-20-6883-2020

Archibald, AT, Neu, JL, Elshorbany, Y, Cooper, OR, Young, PJ, Akiyoshi, H, Cox, RA, Coyle, M, Derwent, R, Deushi, M, Finco, A, Frost, GJ, Galbally, IE, Gerosa, G, Granier, C, Griffiths, PT, Hossaini, R, Hu, L, Jöckel, P, Josse, B, Lin, MY, Mertens, M, Morgenstern, O, Naja, M, Naik, V, Oltmans, S, Plummer, DA, Revell, LE, Saiz-Lopez, A, Saxena, P, Shin, YM, Shaahid, I, Shallcross, D, Tilmes, S, Trickl, T, Wallington, TJ, Wang, T, Worden, HM, Zeng, G. (2020) Tropospheric ozone assessment report: A critical review of changes in the tropospheric ozone burden and budget from 1850 to 2100. Elem Sci Anth. 8:1, doi: 10.1525/elementa.2020.034

Badia, A., Iglesias-Suarez, F., Fernandez, R. P., Cuevas, C. A., Kinnison, D. E., Lamarque, J.-F., Griffiths, P.T., Tarasick, D.W., Liu, J., and Saiz-Lopez, A. (2021). The role of natural halogens in global tropospheric ozone chemistry and budget under different 21st century climate scenarios. J. Geophys. Res.: Atmospheres, 126, e2021JD034859, doi: 10.1029/2021JD034859

Bates, D.R. and M. Nicolet (1950) The photochemistry of atmospheric water vapour, JGR 55(3) 301-327, doi:10.1029/JZ055i003p00301

Bates, K. H., and D. Jacob (2019), An Expanded Definition of the Odd Oxygen Family for Tropospheric Ozone Budgets: Implications for Ozone Lifetime and Stratospheric Influence, Geophys. Res. Lett., 47, doi:10.1029/2019GL084486.

Blum, H. F. (1959) Carcinogenesis by Ultraviolet Light (Princeton, N. J.: Princeton University Press, 1959).

Butler, J. H. (1994) The potential role of the ocean in regulating atmospheric CH3Br. Geophysical Research Letters 21 (3):185-188, doi: 10.1029/94GL00071.

Chameides, W., and J. C. G. Walker, A photochemical theory of tropospheric ozone, J. Geophys. Res., 78, 8751-8760, 1973.

Chapman, S. 1930 A theory of upper-atmosphere ozone. Mem. R. Meteorol. Soc. 3, 103–125.

Danielsen, E.F., (1968) Stratospheric-tropospheric exchange based on radio-activity, ozone and potential vorticity, J. Atmos. Sci. 25() 502-518, https://doi.org/10.1175/1520-0469(1968)025%3C0502:STEBOR%3E2.0.CO;2

Fishman, J. and P. J. Crutzen (1978) The origin of ozone in the troposphere, Nature, 274, 855-858.

Follows, M. J., and J. F. Austin (1992) A zonal average model of the stratospheric contributions to the tropospheric ozone budget, J. Geophys. Res., 97, 18,047-18,060, doi: 10.1029/92JD01834

Griffiths, P. T., Murray, L. T., Zeng, G., Shin, Y. M., Abraham, N. L., Archibald, A. T., Deushi, M., Emmons, L. K., Galbally, I. E., Hassler, B., Horowitz, L. W., Keeble, J., Liu, J., Moeini, O., Naik, V., O'Connor, F. M., Oshima, N., Tarasick, D., Tilmes, S., Turnock, S. T., Wild, O., Young, P. J., and Zanis, P. (2021) Tropospheric ozone in CMIP6 simulations, Atmos Chem Phys, 21, 4187-4218, 10.5194/acp-21-4187-2021, 2021.

Haagen-Smit, A. J. (1952) Chemistry and Physiology of Los Angeles Smog, Ind. Eng. Chem., 44(6), 1342.

Haagen-Smit, A.J. and Fox, M.M. (1955) Automobile Exhaust and Ozone Formation, SAE Transactions Vol. 63 (1955), pp. 575-580 (6 pages), https://www.jstor.org/stable/44468592

Hegglin, M. I. and Shepherd, T. G. (2009) Large climate-induced changes in ultraviolet index and stratosphere-to- troposphere ozone flux, Nat. Geosci., 2, 687–691,doi: 10.1038/ngeo604

Holmes, C.D., M. J. Prather, A.O. Søvde, G. Myhre (2013) Future methane, hydroxyl, and their uncertainties: key climate and emission parameters for future predictions, Atmos. Chem. Phys., 13, 285–302, doi:10.5194/acp-13-285-2013

Holmes, C.D., M. J. Prather, and G. C. M. Vinken (2014) The climate impact of ship NOx emissions: an improved estimate accounting for plume chemistry, Atmos. Chem. Phys., 14, 6801–6812, doi:10.5194/acp-14-6801-2014

Hsu, J., M. J. Prather (2009), Stratospheric variability and tropospheric ozone, J. Geophys. Res., 114, D06102, doi:10.1029/2008JD010942

Hsu, Juno and M. J. Prather (2010), Global long-lived chemical modes excited in a 3-D chemistry transport model: Stratospheric N2O, NOy, O3 and CH4 chemistry, Geophys. Res. Lett., 37, L07805, doi:10.1029/2009GL042243.

Isaksen, I.S.A. and Hov, Ø. (1987) Calculation of trends in the tropospheric concentration of O_3, OH, CO, CH_4 and NOx, Tellus B, 39B(3), 271-285, doi: 10.1111/j.1600-0889.1987.tb00099.x

Johnston, H.S. (1971) Reduction of stratospheric ozone by nitrogen oxide catalysts from supersonic transport exhaust, Science 173 , 517-522, doi: 10.1126/science.173.3996.517

Junge, C.E. (1962) Global ozone budget and exchange between stratosphere and troposphere, Tellus, 14, 363-377, doi: 10.1111/j.2153-3490.1962.tb01349.x

Kleinman, L. I., P. H. Daum, Y.-N. Lee, L. J. Nunnermacker, S. R. Springston, J. Weinstein-Lloyd, and J. Rudolph (2002) Ozone production efficiency in an urban area, J. Geophys. Res., 107(D23), 4733, doi:10.1029/2002JD002529

Lee, D.S., Fahey, D.W., Skowron, A., Allen, M.R., Burkhardt, U., Chen, Q., Doherty, S.J., Freeman, S., Forster, P.M., Fuglestvedt, J., Gettelman, A., De León, R.R., Lim, L.L., Lund, M.T., Millar, R.J., Owen, B., Penner, J.E., Pitari, G., Prather, M.J., Sausen, R., Wilcox, L.J. (2020) The contribution of global aviation to anthropogenic climate forcing for 2000 to 2018, Atmospheric Environment, doi: 10.1016/j.atmosenv.2020.117834

Levy, H. II, (1972) Photochemistry of the lower troposphere, Planet. Spa. Sci., 20(6), 919-935, doi: 10.1016/0032-0633(72)90177-8

Logan, J.A., M.J. Prather, S.C. Wofsy, and M.B. McElroy (1981) Tropospheric chemistry: a global perspective. J. Geophys. Res. 86, 7210-7254, doi: 10.1029/JC086iC08p07210

Mazzuca, G. M., Ren, X., Loughner, C. P., Estes, M., Crawford, J. H., Pickering, K. E., Weinheimer, A. J., and Dickerson, R. R. (2016) Ozone production and its sensitivity to NO_x and VOCs: results from the DISCOVER-AQ field experiment, Houston 2013, Atmos. Chem. Phys., 16, 14463–14474, doi: 10.5194/acp-16-14463-2016

McLinden, C., S. Olsen, B. Hannegan, O. Wild, M. Prather, and J. Sundet (2000) Stratospheric ozone in 3-D models: a simple chemistry and the cross-tropopause flux, J. Geophys. Res., 105, 14653-14665.

Meul, S., Langematz, U., Kröger, P., Oberländer-Hayn, S., and Jöckel, P.: Future changes in the stratosphere-to-troposphere ozone mass flux and the contribution from climate change and ozone recovery, Atmos. Chem. Phys., 18, 7721–7738, doi: 10.5194/acp-18-7721-2018

Molina, M.J. and F.S. Rowland (1974) Stratospheric sink for chlorofluoromethanes: chlorine atom-catalysed destruction of ozone, Nature, 249, 810-812, doi:

Murphy, D. M. and Fahey, D. W. (1994) An estimate of the flux of stratospheric reactive nitrogen and ozone into the troposphere, J. Geophys. Res., 99, 5325–5332, 1994.

Nicolet, M. (1975), Stratospheric ozone: An introduction to its study, Reviews of Geophysics, 13(5) 593-636, doi: 10.1029/RG013i005p00593

Olsen, S. C., C. A. McLinden, and M. J. Prather (2001) The Stratospheric NOy-N2O System: Testing uncertainties in a 3-D framework, J. Geophys. Res., 106(D22), 28771-28784.

Prather, M.J. (1994) Lifetimes and eigenstates in atmospheric chemistry, Geophys. Res. Lett., 21, 801-804, doi: 10.1029/94GL00840

Prather, M.J. (1996) Natural modes and time scales in atmospheric chemistry: theory, GWPs for CH4 and CO, and runaway growth, Geophys.Res.Lett., 23, 2597-2600, doi: 10.1029/96GL02371

Prather, M.J. (1997) Time scales in atmospheric chemistry: CH3Br, the ocean, and ODPs, Glob. Biogeo Cycles, 11, 393-400, doi: /10.1029/97GB01055

Prather, M.J. (2007) Lifetimes and time-scales in atmospheric chemistry, Phil. Trans. R. Soc., A 365: 1705–1726, doi: 10.1098/rsta.2007.2040

Prather, M. J., Ehhalt, D., Dentener, F., Derwent, R., Dlugokencky, E., Holland, E., Isaksen, I., Karima, J., Kirchhoff, V., and Matson, P. (2001). Atmospheric chemistry and greenhouse gases. In J. T. Houghton, Y. Ding, D. J. Griggs, M. Noguer, P. J. van der Linden, P. J. Daix, K. Maskell, and C. A. Johnson (Eds.), Climate change 2001: The scientific basis. Contribution of Working Group I to the Third Assessment Report of the Intergovernmental Panel on Climate Change pp. 239–289). Cambridge, UK: Cambridge University Press.

Prather, M.J. and J. Hsu (2010), Coupling of nitrous oxide and methane by global atmospheric chemistry, Science, 330: 952-954, doi: 10.1126/science.1196285

Prather, M.J., X. Zhu, Q. Tang, J. Hsu, J.L. Neu (2011), An atmospheric chemist in search of the tropopause, J. Geophys. Res., 116: D04306, doi:10.1029/2010JD014939.

Prather, M. J., Zhu, X., Flynn, C. M., Strode, S. A., Rodriguez, J. M., Steenrod, S. D., Liu, J., Lamarque, J.-F., Fiore, A. M., Horowitz, L. W., Mao, J., Murray, L. T., Shindell, D. T., and Wofsy, S. C. (2017) Global atmospheric chemistry – which air matters, Atmos. Chem. Phys., 17, 9081–9102, doi: 10.5194/acp-17-9081-2017

Prather, M. J., Guo, Hao and Zhu, Xin (2023) Deconstruction of tropospheric chemical reactivity using aircraft measurements: the ATom data, Earth Syst. Sci. Data, 15, 3299–3349, doi: 10.5194/essd-15-3299-2023

Prather, Michael (2024). Lifetimes and timescales of tropospheric ozone: Ozone emission experiments [Dataset]. Dryad. https://doi.org/10.5061/dryad.qbzkh18qq

Roelofs, G. J. and Lelieveld, J. O. S.: Model study of the influence of cross-tropopause O3 transports on tropospheric O3 levels, Tellus B, 49, 38–55, doi: 10.3402/tellusb.v49i1.15949, 1997.

Roffo, A. H. (1939) Ueber die physikalisch-chemische Aetiologie der Krebskrankheit, Strahlentherapie 66:328-350.

Ruiz, D. J. and Prather, M. J. (2022) From the middle stratosphere to the surface, using nitrous oxide to constrain the stratosphere–troposphere exchange of ozone, Atmos. Chem. Phys., 22, 2079–2093, doi: 10.5194/acp-22-2079-2022

Stevenson, D. S., Young, P. J., Naik, V., Lamarque, J. F., Shindell, D. T., Voulgarakis, A., Skeie, R. B., Dalsoren, S. B., Myhre, G., Berntsen, T. K., Folberth, G. A., Rumbold, S. T., Collins, W. J., MacKenzie, I. A., Doherty, R. M., Zeng, G., van Noije, T. P. C., Strunk, A., Bergmann, D., Cameron-Smith, P., Plummer, D. A., Strode, S. A., Horowitz, L., Lee, Y. H., Szopa, S., Sudo, K., Nagashima, T., Josse, B., Cionni, I., Righi, M., Eyring, V., Conley, A., Bowman, K. W., Wild, O., and Archibald, A., (2013), Tropospheric ozone changes, radiative forcing and attribution to emissions in the Atmospheric Chemistry and Climate Model Intercomparison Project (ACCMIP), Atmos Chem Phys, 13, 3063-3085, 10.5194/acp-13-3063-2013

Szopa, S., Naik, V., Adhikary, B., Artaxo, P., Berntsen, T., Collins, W. D., et al. (2021) Short-Lived Climate Forcers. In Climate Change 2021: The Physical Science Basis. Contribution of Working Group I to the Sixth Assessment Report of the Intergovernmental Panel on Climate Change [Masson-Delmotte, V., Zhai, P., Pirani, A., Connors, S.L., Péan, P.C., Berger, S. et al. (eds.)]. Cambridge University Press, Cambridge, United Kingdom and New York, NY, USA, pp. 817–922, doi:10.1017/9781009157896.008

Tang, Qi and M.J. Prather (2012), Five blind men and the elephant: what can the NASA Aura ozone measurements tell us about stratosphere-troposphere exchange? Atmos. Chem. Phys., 12, 2357–2380, doi: 10.5194/acp-12-2357-2012

Thrush, B. A. (1980) The Chemistry of the Stratosphere, Philosophical Transactions of the Royal Society of London. Series A, Mathematical and Physical Sciences Vol. 296, No. 1418, The Middle Atmosphere as Observed form Balloons, Rockets and Satellites (Mar. 6, 1980), pp. 149-160 (12 pages))

Wang, M. and Fu, Q. (2023). Changes in stratosphere-troposphere exchange of air mass and ozone concentration in CCMI models from 1960 to 2099. Journal of Geophysical Research: Atmospheres, 128, e2023JD038487, doi: 10.1029/2023JD038487

Wild, O. and M.J. Prather (2006) Global tropospheric ozone modeling: Quantifying errors due to grid resolution, J. Geophys. Res., 111(D11), D11305, doi:10.1029/2005JD006605.

Wild, O., J.K. Sundet, M.J. Prather, I.S.A. Isaksen, H. Akimoto, E.V. Browell, and S.J. Oltmans (2003) Chemical transport model ozone Simulations for spring 2001 over the western Pacific: Comparisons with TRACE-P lidar, ozonesondes and TOMS columns, J. Geophys. Res., 108(D21), 8826, doi:10.1029/2002JD003283.

Williams, R. S., Hegglin, M. I., Kerridge, B. J., Jöckel, P., Latter, B. G., and Plummer, D. A. (2019) Characterising the seasonal and geographical variability in tropospheric ozone, stratospheric influence and recent changes, Atmos. Chem. Phys., 19, 3589–3620, doi: 10.5194/acp-19-3589-2019

WMO (2022) World Meteorological Organization (WMO). Executive Summary. Scientific Assessment of Ozone Depletion: 2022, GAW Report No. 278, 56 pp.; WMO: Geneva, 2022, https://library.wmo.int/idurl/4/42105

Young, P. J., Naik, V., Fiore, A. M., Gaudel, A., Guo, J., Lin, M. Y., Neu, J. L., Parrish, D. D., Rieder, H. E., Schnell, J. L., Tilmes, S., Wild, O., Zhang, L., Ziemke, J., Brandt, J., Delcloo, A., Doherty, R. M., Geels, C., Hegglin, M. I., Hu, L., Im, U., Kumar, R., Luhar, A., Murray, L., Plummer, D., Rodriguez, J., Saiz-Lopez, A., Schultz, M. G., Woodhouse, M. T., and Zeng, G., (2018) Tropospheric Ozone Assessment Report: Assessment of global-scale model performance for global and regional ozone distributions, variability, and trends, Elementa-Science of the Anthropocene, 6, doi: 10.1525/elementa.265

Ziemke, J. R., S. Chandra, B. N. Duncan, L. Froidevaux, P. K. Bhartia, P. F. Levelt, and J. W. Waters (2006) Troposphericozone determined from Aura OMI and MLS: Evaluation of measurements and comparison with the Global Modeling Initiative's Chemical Transport Model,J. Geophys. Res.,111, D19303, doi:10.1029/2006JD007089

Ziemke, J. R. and Chandra, S. (2012) Development of a climate record of tropospheric and stratospheric column ozone from satellite remote sensing: evidence of an early recovery of global stratospheric ozone, Atmos. Chem. Phys., 12, 5737–5753, https://doi.org/10.5194/acp-12-5737-2012